Peer-Reviewed Technical Communication

Bayesian Iterative Channel Estimation and Turbo Equalization for Multiple-Input–Multiple-Output Underwater Acoustic Communications

Xiangzhao Qin, *Student Member, IEEE*, Fengzhong Qu ⓘ, *Senior Member, IEEE*, and Yahong Rosa Zheng, *Fellow, IEEE*

Abstract—This article investigates a robust receiver scheme for a single carrier, multiple-input–multiple-output (MIMO) underwater acoustic (UWA) communications, which uses the sparse Bayesian learning algorithm for iterative channel estimation embedded in Turbo equalization (TEQ). We derive a block-wise sparse Bayesian learning framework modeling the spatial correlation of the MIMO UWA channels, where a more robust expectation–maximization algorithm is proposed for updating the joint estimates of channel impulse response, residual noise, and channel covariance matrix. By exploiting the spatially correlated sparsity of MIMO UWA channels and the second-order *a priori* channel statistics from the training sequence, the proposed Bayesian channel estimator enjoys not only relatively low complexity but also more stable control of the hyperparameters that determine the channel sparsity and recovery accuracy. Moreover, this article proposes a low complexity space-time soft decision feedback equalizer (ST-SDFE) with successive soft interference cancellation. Evaluated by the undersea 2008 Surface Processes and Acoustic Communications Experiment, the improved sparse Bayesian learning channel estimation algorithm outperforms the conventional Bayesian algorithms in terms of the robustness and complexity, while enjoying better estimation accuracy than the orthogonal matching pursuit and the improved proportionate normalized least mean squares algorithms. We have also verified that the proposed ST-SDFE TEQ significantly outperforms the low-complexity minimum mean square error TEQ in terms of the bit error rate and error propagation.

Index Terms—Channel estimation (CE), multiple-input–multiple-output (MIMO), space-time soft decision feedback equalizer (ST-SDFE), sparse Bayesian learning (SBL), successive soft interference cancellation (SSIC), Turbo equalization (TEQ), underwater acoustic (UWA) communications.

I. INTRODUCTION

UNDERWATER acoustic (UWA) communications exhibit significant technical challenges due to the following three main reasons.

1) The channel impulse response (CIR) extends excessive multipath delay spread which results in severe intersymbol interference that is across hundreds of symbol periods.

X. Qin and F. Qu are with the Key Laboratory of Ocean Observation-Imaging Testbed of Zhejiang Province, Zhejiang University, Zhoushan 316021, China (e-mail: chrisqinxz@zju.edu.cn; jimqufz@zju.edu.cn).
Y. R. Zheng is with the Department of Electrical and Computer Engineering, Lehigh University, Bethlehem, PA 18015-3084 USA (e-mail: yrz218@lehigh.edu).

2) Significant time variation and Doppler spread due to dynamic fluctuations of wavefront and motion of the transceiver platforms obstruct channel capability and impair the reliability of coherent phase detection.

3) The available channel bandwidth is very limited due to the frequency-dependent energy loss at high frequency, which makes high data rate UWA communications difficult [1].

To realize high data rate communication in UWA channels, multiple-input–multiple-output (MIMO) schemes are considered a viable solution thanks to the temporal and spatial diversity gains of MIMO system. In the past two decades, extensive research on MIMO UWA communications has ranged from single carrier [2]–[11] to multicarrier [12]–[15] coherent modulation systems. However, MIMO schemes under UWA channels still encounter several obstacles. For example, strong spatial correlation decreases the diversity, and MIMO co-channel interference (CCI) overwhelms receiver processing, especially in the fast time-varying channels. Therefore, MIMO UWA transceivers often require accurate channel estimation (CE), powerful equalization, and decoding schemes to achieve satisfactory performance.

Currently, two equalization approaches are commonly used in UWA communications, namely the CE-based equalization and the direct adaption (DA)-based equalization. The DA-based equalizers calculate the adaptive equalization filters directly without explicitly estimating the channel coefficients, which often requires longer training sequence to reach convergence [16]. In contrast, the CE-based methods explicitly estimate the channel coefficients and design the equalizer filters accordingly via the training sequence [17]. While exposing higher computational complexity than the DA-based equalizers, the CE-based approaches require shorter training sequence and achieve better performance than the DA-based equalizer.

UWA channels tend to be sparse both in the Doppler-spread and delay-spread domains, which motivates several sparse CE and fast tracking methods. The classic least mean squares [18] and its proportionate variations [19], [20] have been applied to UWA communications [21], [22] successfully with variable step sizes and data reuse to combat the slow convergence. Another approach is the L_p-norm regularized optimization method [23]–[25], where p is a fractional number between 0 and 2. When $p = 1$, minimizing the L_1-norm of the error function leads to the sign algorithm. More recently, the compressed sensing approach which utilizes the mixed L_1- and L_2-norms [26], [27] has been applied to UWA CE where the dictionary is defined in the space-time domain. Although these methods are effective, they often require the sparse structure of CIR to remain stationary over the length of a data block, where this constraint is easily violated by the dynamic underwater environment. An alternative approach to alleviating the time variation of the CIR is to estimate the delay-Doppler-spread function of sparse arrivals, which is far less restrictive than assuming the constant

CIR [28], [29], but this method harvests little gain when compared with the high computational complexity which is not preferable, especially for MIMO channels. Moreover, much more effort focuses on how to exploit the channel sparseness, and there is little research that works on the spatial correlation property of the MIMO UWA channels.

Recently, the Bayesian iterative learning method has been applied to UWA CE [30] and passive source localization [31], [32]. These methods were originally proposed for estimating the single measurement vector or the multiple measurement vector [33]–[35]. By incorporating the knowledge of hierarchically underlying models and the *a priori* information into the estimation process, Bayesian estimation shows its superiority in terms of solving the channel overparametrization problem. However, Bayesian estimation exhibits huge computational complexity when the channel length or the number iteration is large or when the MIMO UWA channels are spatially correlated. Simplification is often used in practice, which assumes that the channel covariance matrix is diagonal. Meanwhile, this assumption is invalid in terms of the MIMO UWA channels.

This article proposes an improved sparse Bayesian learning (I-SBL) algorithm for MIMO UWA CE by exploiting the spatial correlation structure and the temporal sparsity of the MIMO UWA channels simultaneously. The proposed I-SBL models the MIMO channel covariance matrix as block diagonal with each subblock capturing the spatial correlation of the MIMO channel and different subblocks corresponding to the temporal delay taps. I-SBL also characterizes the temporal sparsity of the MIMO channels via the gains of the subblocks of the covariance matrix. A sparsity controlling factor γ is used to determine the sparsity of I-SBL, which sets the subblock of the covariance matrix to zeros if the gain of the subblock is smaller than γ. The proposed I-SBL algorithm uses the expectation–maximization (EM) algorithm to update the hyperparameters and is further enhanced via the initialization of the channel covariance matrix and noise power from the training sequence. In the iterative EM algorithm, when γ_l is less than a fixed value γ, the corresponding entries of the given structured MIMO channel vector $\mathbf{h}_m$ are removed, reinforcing the sparsity of the spatially correlated channels. The estimated channel coefficients are then applied to a Turbo equalization (TEQ) unit with a simplified space-time soft decision feedback equalizer (ST-SDFE), achieving successive soft interference cancellation (SSIC).

The overall receiver scheme was tested by the field trial data collected undersea during the 2008 Surface Process and Acoustic Communications Experiment (SPACE08) where the transmitted signal was designed by the Missouri University of Science and Technology [17]. The experimental results demonstrate that the proposed I-SBL has higher complexity than the improved proportionate normalized least mean square (IPNLMS) algorithm, but achieves faster parameter convergence and enjoys lower computational complexity than the conventional Bayesian algorithms. Moreover, the ST-SDFE-based TEQ in combination with the I-SBL CE algorithm outperforms the low-complexity minimum mean square error (LC-MMSE) TEQ significantly in terms of bit error rate (BER). Complexity analysis also shows that I-SBL has an acceptable complexity for practical implementation.

Notations: Upper (lower) boldface letters are used for matrices (column vectors). $(\cdot)^H$, $(\cdot)^T$, and $(\cdot)^*$ represent the Hermitian, transposition, and conjugation, respectively. Operator $\mathbf{E}[\cdot]$ represents the statistical expectation and $\otimes$ is the Kronecker product. Symbol $\mathbf{I}_L$ denotes the identity matrix with size $L \times L$. When the dimension is evident from the context, for simplicity, we just use $\mathbf{I}$. Vector norms: $\| \cdot \|^2$ is the squared Frobenius norm of a vector or a matrix, and $\| \cdot \|_1$ and $\| \cdot \|_0$ are the L_1- and L_0-norms of a vector, respectively. The $i \times j$ complex matrix space is represented by $\mathcal{C}^{i \times j}$. The matrix $\text{diag}\{d_1, d_2, \ldots, d_j\}$ is a $j \times j$ diagonal matrix with diagonal elements
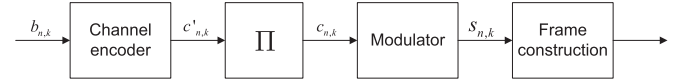

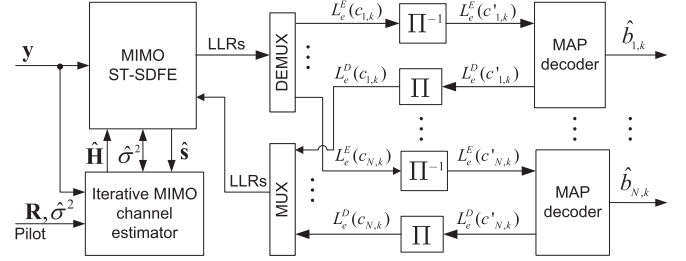Fig. 1. Encoding scheme on the nth transmit branch, where Π denotes the interleaver.

Fig. 2. Proposed MIMO detector using Bayesian iterative CE and TEQ.

$d_1, d_2, \ldots, d_j$, and similarly Bdiag$\{\cdot\}$ is a block diagonal matrix. Other mathematical symbols are defined after their first appearance.

II. SYSTEM DESCRIPTION

Consider an $N \times M$ MIMO UWA communication system, where N and M are the numbers of transducers and hydrophones, respectively. At the transmitter side, each bit stream is independently encoded, interleaved, modulated, and then transmitted by a transducer via a frame construction unit. Fig. 1 depicts the encoding scheme of the nth transmit branch, with $b_{n,k}$, $c'_{n,k}$, $c_{n,k}$, and $s_{n,k}$ being the information bit, the encoded bit, the interleaved bit, and the modulated symbol, respectively.

For example, the SPACE08 experiment adopts a rate-1/2 nonsystematic convolutional code with a generator polynomial $[G_1, G_2] = [17, 13]_{\text{oct}}$ and a random interleaver Π. The bit to symbol employs QPSK, 8PSK, and 16QAM with the constellation sizes being $Q = 4, 8$, and 16, respectively, where each of the constellation set $\mathcal{S} = \{\chi_q\}_{q=1}^Q$ carries $\log_2 Q$ bits, i.e., the bit patterns $\{c_{n,p}^k = c_{n,(k-1)\log_2 Q+p}\}_{p=1}^{\log_2 Q}$ are mapped to symbol $s_{n,k}$.

Fig. 2 depicts the structure of the proposed iterative MIMO CE and TEQ, where $\mathbf{y}$ denotes the received sampling vector of the M received branches. The training sequence of the received $\mathbf{y}$ is used for calculating $\mathbf{R}$ and $\hat{\sigma}^2$ that are the second-order *a priori* statistics of the UWA channels. The iterative MIMO channel estimator unit provides the estimates of channel matrix $\hat{\mathbf{H}}$ and the noise variance $\hat{\sigma}^2$ for the MIMO ST-SDFE unit, where $L_e^E(c_{n,k})$ and $L_e^D(c_{n,k})$ denote the extrinsic log-likelihood ratios (LLRs) of the MIMO ST-SDFE unit and the maximum *a posteriori* probability (MAP) decoder, respectively, with k being the index of the encoded bit and n being the index of the transducer. The MIMO ST-SDFE calculates the extrinsic LLRs $L_e^E(c_{n,k})$, which are then regrouped via the DEMUX and deinterleaver (Π^{-1}) to form the a priori LLRs $L_e^E(c'_{n,k})$ for the MAP decoder. The MAP decoder calculates the bit extrinsic LLRs $L_e^D(c'_{n,k})$, which are then fed back to the MIMO ST-SDFE as the *a priori* LLRs $L_e^D(c_{n,k})$ via interleaver (Π) for the next Turbo iteration. Meanwhile, the MIMO ST-SDFE feeds the estimated symbols $\hat{\mathbf{s}}$ and the reestimated noise variance $\hat{\sigma}^2$ into the MIMO channel estimator for the decision-directed (DD) CE.

To combat the time-varying fading in UWA channels, the MIMO detector partitions each large data block into smaller sized subblocks. Fig. 3 describes the detector partition prepared for the MIMO CE unit and the MIMO ST-SDFE unit, which divides the data block into several blocks of length N_b; each block is further divided into smaller
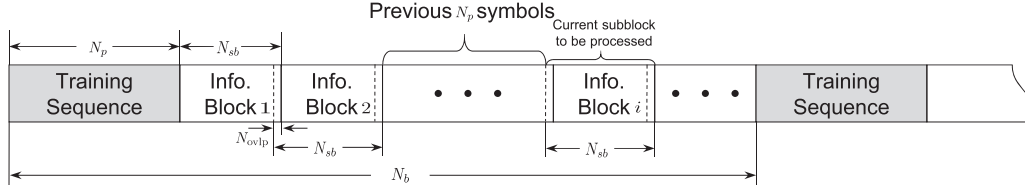
Fig. 3. Partition of the transmitted frame at the receiver: Training sequence and data payload in subblocks [22].

subblocks of length N_{sb}. Each subblock is prevented by an overlap of length N_{ovlp}, and the equalized symbols at the tail of previous subblock are equalized again at the current sequential subblock. In this way, performance degradation in the tail symbols of each subblock is prevented. The previous N_p symbols can be the training symbols or the detected symbols from the equalizer of the previous subblocks.

The proposed CE works in two modes: the training mode and the DD mode. In the training mode, the MIMO detector uses the training symbols for CE in the first subblock. In the DD mode, the previously detected symbols or a combination of partial training symbols are used for CE for the second and subsequent subblocks. The algorithm outline of the subblock processing has been discussed in [22], which is out of the scope of this article.

III. ITERATIVE MIMO CE AND TEQ

After front-end processing which includes frame synchronization, Doppler shift estimation, and waveform resampling, the discrete-time baseband signal received at the mth hydrophone is expressed by

$$y_{m,k} = \sum_{n=1}^{N} \sum_{l=0}^{L-1} h_{m,n}(k,l) s_{n,k-l} + w_{m,k} \tag{1}$$

where $s_{n,k-l}$ is the transmitted symbol of the nth transducer, $\{h_{m,n}(k,l)\}_{l=0}^{L-1}$ is the lth channel tap between the nth transducer and the mth hydrophone at time instant k, and $w_{m,k}$ is the zero mean additive white Gaussian noise (AWGN) whose power is assumed to be σ^2.

A. MIMO CE: The I-SBL Algorithm

When the time duration of the training sequence or the previously detected payload sequence $\{x_{n,k}\}_{k=0}^{N_p-1}$ is less than the channel coherence time, the channel coefficients $h_{m,n}(k,l)$ are approximated as quasi time invariant, which is $h_{m,n}(k,l) \approx h_{m,n}(l)$. The received signal at the mth hydrophone corresponding to the transmitted sequence in a matrix form is approximated as

$$\mathbf{y}_m \approx \sum_{l=0}^{L-1} \mathbf{X}_l \mathbf{h}_{m,l} + \mathbf{w}_m = \mathbf{X}\mathbf{h}_m + \mathbf{w}_m \tag{2}$$

where

$$\mathbf{y}_m \triangleq \left[y_{m,L-1}, y_{m,L}, \ldots, y_{m,N_p-1}\right]^T \in \mathcal{C}^{(N_p-L+1)\times 1}$$

$$\mathbf{h}_{m,l} \triangleq [h_{m,1}(l), h_{m,2}(l), \ldots, h_{m,N}(l)]^T \in \mathcal{C}^{N\times 1}$$

$$\mathbf{w}_m \triangleq \left[w_{m,L-1}, w_{m,L}, \ldots, w_{m,N_p-1}\right]^T \in \mathcal{C}^{(N_p-L+1)\times 1}$$

$$\mathbf{h}_m \triangleq \left[\mathbf{h}_{m,0}^T, \mathbf{h}_{m,1}^T, \ldots, \mathbf{h}_{m,L-1}^T\right]^T \in \mathcal{C}^{NL\times 1}.$$

Matrix $\mathbf{X}_l \in \mathcal{C}^{(N_p-L+1)\times N}$ is defined as

$$\mathbf{X}_l \triangleq \begin{bmatrix} x_{1,L-l-1} & x_{2,L-l-1} & \cdots & x_{N,L-l-1} \\ x_{1,L-l} & x_{2,L-1} & \cdots & x_{N,L-l} \\ \vdots & \vdots & \vdots & \vdots \\ x_{1,N_p-l-1} & x_{2,N_p-l-1} & \cdots & x_{N,N_p-l-1} \end{bmatrix} \tag{3}$$

and matrix $\mathbf{X}$ is concatenated as $\mathbf{X} = [\mathbf{X}_0, \mathbf{X}_1, \ldots, \mathbf{X}_{L-1}] \in \mathcal{C}^{(N_p-L+1)\times NL}$.

The equivalent input and output (I/O) model in (2) differs from the conventional system I/O model for block-wise MMSE CE, where we concatenate the lth channel coefficients of all the N transducers as one subgroup $\mathbf{h}_{m,l}$, while the conventional MIMO channel model concatenates the L channel taps of each (m, n)-pair of transmitter and receiver. The modified I/O model (2) ensures that the spatial correlation of the MIMO UWA channels is utilized easily. Besides, the UWA channels are usually sparse in time. Although $\mathbf{h}_m$ contains NL unknowns, many entries of $\mathbf{h}_m$ are approximately zero and the sparseness is usually similar across the N transducers. When the length of the training symbols $(N_p - L + 1) < (NL)$, the system equation (2) is under determined or the estimation of $\mathbf{h}_m$ is overparameterized, and shall be avoided. Moreover, for the (m, n)th pair of transmit–receive elements, the signals of the other $(N-1)$ channel are mixed in the received samples, which will induce estimation ambiguity due to spatial correlation. These aspects lead to formidable difficulties for the conventional Bayesian learning algorithms to estimate the MIMO UWA channels. This article improves the sparse Bayesian Learning (SBL) algorithm by reducing the computational complexity and improving the estimation accuracy. In the EM iteration, the E-step yields the expectation of $\mathbf{h}_m$ and the hyperparameters are obtained in the M-step.

1) EM Algorithm E-Step: The E-step takes the expectation of the *a posteriori* likelihood as the estimate result for the MIMO UWA channels whose Bayesian hierarchy is modeled as

$$\Pr(\mathbf{h}_m|\mathbf{y}_m; \mathbf{R}_m, \sigma^2) = \frac{p(\mathbf{y}_m|\mathbf{h}_m; \sigma^2)\Pr(\mathbf{h}_m; \mathbf{R}_m)}{\sum_{\mathbf{h}_m} p(\mathbf{y}_m|\mathbf{h}_m; \sigma^2)\Pr(\mathbf{h}_m; \mathbf{R}_m)} \tag{4}$$

where the conditional Gaussian likelihood is

$$p(\mathbf{y}_m|\mathbf{h}_m; \sigma^2) \sim \mathcal{CN}(\mathbf{X}\mathbf{h}_m, \sigma^2\mathbf{I}) \tag{5}$$

and the a *priori* likelihood of $\Pr(\mathbf{h}_m; \mathbf{R}_m)$ is

$$p(\mathbf{h}_m; \mathbf{R}_m) \sim \mathcal{CN}(\mathbf{0}, \mathbf{R}_m) \tag{6}$$

where $\mathbf{R}_m$ is the hidden hyperparameter incorporated inside the hierarchical model. For the conventional Bayesian algorithm, $\mathbf{R}_m$ is just considered as the uncorrelated diagonal matrix. As we consider the MIMO UWA channel $\mathbf{h}_m$ to be spatially correlated and sparse, $\mathbf{R}_m$ is rewritten as

$$\mathbf{R}_m = \text{Bdiag}\{\gamma_0 \boldsymbol{\Delta}_0, \ldots, \gamma_{L-1} \boldsymbol{\Delta}_{L-1}\} \tag{7}$$

with $\{\boldsymbol{\Delta}_l\}_{l=0}^{L-1}$ being the covariance submatrix that determines the spatial correlation of the lth tap and γ_l being the hyperparameter that controls the channel sparsity. When $\gamma_l = 0$, the corresponding $\mathbf{X}_l$ becomes zero and is then discarded from matrix $\mathbf{X}$. In this way, the sparsity of MIMO channel is controlled jointly thanks to the spatial correlation of UWA channels. To avoid overfitting, we update the hidden hyperparameters γ_l and $\boldsymbol{\Delta}_l$ instead of updating $\mathbf{R}_m$ directly. Since all the $\boldsymbol{\Delta}_l$ are assumed to be identically distributed, we consider using one positive–definite matrix $\boldsymbol{\Delta}$ to model all the $\boldsymbol{\Delta}_l$. Thus, (6) becomes $\mathbf{R}_m = \boldsymbol{\Gamma} \otimes \boldsymbol{\Delta}$ with $\boldsymbol{\Gamma} \triangleq \mathrm{diag}\{\gamma_0, \ldots, \gamma_{L-1}\}$. The *a priori* likelihood $p(\mathbf{h}_m; \mathbf{R}_m) \triangleq p(\mathbf{h}_m; \gamma_l, \boldsymbol{\Delta})$. Using the Bayesian rule, we obtain the *a posteriori* likelihood of $\mathbf{h}_m$, which is also the Gaussian process

$$p(\mathbf{h}_m | \mathbf{y}_m; \mathbf{R}_m, \sigma^2) \sim \mathcal{CN}(\boldsymbol{\mu}, \boldsymbol{\Xi}) \tag{8}$$

with the mean

$$\boldsymbol{\mu} = (\sigma^2)^{-1} \boldsymbol{\Xi} \mathbf{X}^H \mathbf{y}_m \tag{9}$$

and the covariance matrix

$$\boldsymbol{\Xi} = \left(\mathbf{R}_m^{-1} + (\sigma^2)^{-1} \mathbf{X}^H \mathbf{X}\right)^{-1}. \tag{10}$$

Therefore, given all the hyperparameters $\boldsymbol{\Theta} = \{\gamma_l, \boldsymbol{\Delta}, \sigma^2\}$ acquired from the previous EM iteration, the MAP estimate of $\mathbf{h}_m$ is given by the E-step

$$\hat{\mathbf{h}}_m \triangleq \boldsymbol{\mu} = \left(\sigma^2 \mathbf{R}_m^{-1} + \mathbf{X}^H \mathbf{X}\right)^{-1} \mathbf{X}^H \mathbf{y}_m. \tag{11}$$

2) EM Algorithm M-Step: The M-step maximizes the likelihood $p(\mathbf{y}_m; \boldsymbol{\Theta})$ to update the hyperparameter set $\boldsymbol{\Theta}$. This is equivalent to minimizing $-\log p(\mathbf{y}_m; \boldsymbol{\Theta})$, yielding the effective cost function

$$\mathcal{L}(\boldsymbol{\Theta}) \triangleq -2 \log \sum_{\mathbf{h}_m} \left(p(\mathbf{y}_m | \mathbf{h}_m; \sigma^2) \, p(\mathbf{h}_m; \gamma_l, \boldsymbol{\Delta})\right)$$

$$= \mathbf{y}_m^H \left(\boldsymbol{\Xi}\right)^{-1} \mathbf{y}_m + \log |\boldsymbol{\Xi}| \tag{12}$$

with $\boldsymbol{\Xi} \triangleq \sigma^2 \mathbf{I} + \mathbf{X} \mathbf{R}_m \mathbf{X}^H$. The EM formulation then treats the $\mathbf{h}_m$ as hidden parameters and takes the partial derivative of $\mathcal{L}(\boldsymbol{\Theta})$ with respect to $\{\gamma_l, \boldsymbol{\Delta}, \sigma^2\}$ leading to zero. To estimate $\boldsymbol{\gamma} \triangleq [\gamma_0, \ldots, \gamma_{L-1}]$ and $\boldsymbol{\Delta}$, we notice that the conditional likelihood $p(\mathbf{y}_m | \mathbf{h}_m; \sigma^2)$ is unrelated to $\boldsymbol{\gamma}$ and $\boldsymbol{\Delta}$. Therefore, the cost function with target $\{\boldsymbol{\gamma}, \boldsymbol{\Delta}\}$ can be simplified to

$$\mathcal{L}(\boldsymbol{\Theta}_{\boldsymbol{\gamma}, \boldsymbol{\Delta}}) \propto -\log \left(|\boldsymbol{\Gamma}|^N |\boldsymbol{\Delta}|^L\right) - \mathrm{Tr} \left[(\boldsymbol{\Gamma} \otimes \boldsymbol{\Delta})^{-1} (\boldsymbol{\Xi} + \mathbf{h}_m \mathbf{h}_m^H)\right]. \tag{13}$$

The derivative of (13) with respect to $\boldsymbol{\Delta}$ and $\{\gamma_l\}_{l=0}^{L-1}$ is given by

$$\boldsymbol{\Delta} = \frac{1}{L_\alpha} \sum_{\forall l: \gamma_l > \gamma} \left(\boldsymbol{\Xi}_l + \mathbf{h}_{m,l} \mathbf{h}_{m,l}^H\right) / \gamma_l \tag{14}$$

$$\gamma_l = \frac{1}{N} \mathrm{Tr} \left[\boldsymbol{\Delta}^{-1} \left(\boldsymbol{\Xi}_l + \mathbf{h}_{m,l} \mathbf{h}_{m,l}^H\right)\right] \tag{15}$$

where L_α is the number of the channel taps that are nonzero over the channel length L at the current EM iteration and γ detailed in the previous section is the threshold that determines the channel sparseness. $\mathrm{Tr}[\cdot]$ denotes the trace of the matrix. We also define

$$\boldsymbol{\Xi}_l \triangleq [\boldsymbol{\Xi}]_{[lN+1:(l+1)N, lN+1:(l+1)N]}.$$

Similarly, the residual noise power σ^2 is solved by setting the partial derivative of $\mathcal{L}(\boldsymbol{\Theta}_{\sigma^2})$ over σ^2 to zero. The solution is obtained as

$$\sigma^2 = \frac{\|\mathbf{y}_m - \mathbf{X} \mathbf{h}_m\|^2 + \hat{\sigma}^2 [NL - \mathrm{Tr}(\boldsymbol{\Xi} \mathbf{R}_m^{-1})]}{N_p - L + 1} \tag{16}$$

Algorithm 1: I-SBL for MIMO UWA CE.

Given number of EM iterations T, the sparsity controlling factor $\gamma = 2 \times 10^{-6}$, the convergence threshold $\delta = 10^{-3}$.

Initialization $t = 0$, $\hat{\mathbf{h}}_m = \mathbf{0}_{NL \times 1}$, $(\sigma^2)^{(0)}$, $\mathbf{R}_m^{(0)}$;

nonzero index $\mathbf{z} = [1, 2, \ldots, L]$;

nonzero dictionary list $\mathbf{q} = [1, 2, \ldots, NL]^T$.

while $t < T$ **do**

  $t \leftarrow t + 1$;

  E-step:

  update $\mathbf{h}_m^{(t)}$ using (11);

  M-step:

  update $\boldsymbol{\Delta}$ and γ_l using (14) and (15), respectively;

  update $\mathbf{R}_m^{(t)}$ using $\mathbf{R}_m^{(t)} = \boldsymbol{\Gamma} \otimes \boldsymbol{\Delta}$;

  update noise power $(\sigma^2)^{(t)}$ using (16).

  if $\min\{|\gamma_l|\} < \gamma, l \in \mathbf{z}$ **then**

    $\mathbf{z} := \forall l \in \mathbf{z}$, such that $|\gamma_l| > \gamma$;

    update $\mathbf{X} \leftarrow [\mathbf{X}]_{[:, (\mathbf{z}-1)N+1:\mathbf{z}N]}$;

    update $\mathbf{q} \leftarrow [\mathbf{q}]_{[(\mathbf{z}-1)N+1:\mathbf{z}N]}$

  end if

  if $\|\mathbf{h}_m^{(t)}\|_0 = \|\mathbf{h}_m^{(t-1)}\|_0$ **then**

    if $\|\mathbf{h}_m^{(t)} - \mathbf{h}_m^{(t-1)}\|_1 / \|\mathbf{h}_m^{(t)}\|_1 \le \delta$ **then**

      break;

    end if

  end if

end while

Output $\hat{\mathbf{h}}_m(\mathbf{q}) \leftarrow \mathbf{h}_m^{(t)}$.

---

where $\hat{\sigma}^2$ on the right-hand side denotes the estimated σ^2, which is estimated from the previous EM iteration. For the derivation of (14)–(16), Zhang and Rao [33] give more theoretical details.

After the tth EM iteration is finished by involving (11) and (14)–(16), we set $t := t + 1$, and repeat EM iteration until t equals T or meets the condition $\|\mathbf{h}_m^{(t)} - \mathbf{h}_m^{(t-1)}\|_1 / \|\mathbf{h}_m^{(t)}\|_1 \le \delta$, where δ is the convergence threshold that determines the accuracy of the estimation results. The I-SBL algorithm for MIMO UWA CE is summarized in Algorithm 1. Note that $\mathbf{R}_m^{(0)}$ is computed using the training sequence and is used for every subblock (N_{sb}-length) throughout the whole data packet, while $\mathbf{h}_m^{(t)}$ and $\mathbf{R}_m^{(t)}$ are updated for each subblock in every EM iteration inside the channel estimator.

B. MIMO TEQ

The proposed MIMO detector uses the TEQ that combines the ST-SDFE simplified from [9] with the MAP decoder. The payload symbols of a subblock are denoted as $\{s_{n,k}(0 \le k \le N_{sb} - 1)\}_{n=1}^N$. Define K_1 and K_2 as the lengths of the noncasual and casual parts of the nonlinear equalizer, respectively. The overall filter length used for the symbol-wise equalization is $K = K_1 + K_2 + 1$. After the interblock interference is removed from the current subblock, the system I/O model is defined as

$$\mathbf{y}^k = \mathbf{H} \mathbf{s}^k + \mathbf{w}^k \tag{17}$$

where the output

$$\mathbf{y}^k \triangleq [\mathbf{y}_{k-K_2}^T, \mathbf{y}_{k-K_2+1}^T, \ldots, \mathbf{y}_{k+K_1}^T]^T \in \mathcal{C}^{MK \times 1}$$

denotes the observation vector for time instant k with

$$\mathbf{y}_k \triangleq [y_{1,k}, y_{2,k}, \ldots, y_{M,k}]^T \in \mathcal{C}^{M \times 1}$$

the input

$$\mathbf{s}^k \triangleq [\mathbf{s}_{k-K_2-L+1}^T, \ldots, \mathbf{s}_{k+K_1}^T]^T \in \mathcal{C}^{N(K+L-1)\times 1}$$

with

$$\mathbf{s}_k \triangleq [s_{1,k}, s_{2,k}, \ldots, s_{N,k}]^T \in \mathcal{C}^{N\times 1}$$

and the concatenated noise vector is expressed as

$$\mathbf{w}^k \triangleq [\mathbf{w}_{k-K_2}^T, \mathbf{w}_{k-K_2+1}^T, \ldots, \mathbf{w}_{k+K_1}^T]^T \in \mathcal{C}^{MK\times 1}$$

with

$$\mathbf{w}_k \triangleq [w_{1,k}, w_{2,k}, \ldots, w_{M,k}]^T \in \mathcal{C}^{M\times 1}.$$

Let $K_3 = K_2 + L - 1$, then the MIMO channel matrix is defined as

$$\mathbf{H} \triangleq \begin{bmatrix} \mathbf{H}_{L-1} & \cdots & \mathbf{H}_0 & \cdots & 0 \\ \vdots & \ddots & \ddots & \ddots & \vdots \\ 0 & \cdots & \mathbf{H}_{L-1} & \cdots & \mathbf{H}_0 \end{bmatrix}$$
$$\in \mathcal{C}^{(MK)\times N(K_3+K_1+1)}$$

with

$$\mathbf{H}_l \triangleq \begin{bmatrix} h_{1,1}(l) & h_{1,2}(l) & \cdots & h_{1,N}(l) \\ \vdots & \vdots & \ddots & \vdots \\ h_{M,1}(l) & h_{M,2}(l) & \cdots & h_{M,N}(l) \end{bmatrix} \in \mathcal{C}^{M\times N}. \quad (18)$$

The channel equalizer is to equalize the payload symbols $\{s_{n,k}(0 \le k \le N_{sb}-1)\}_{n=1}^N$ given the observation signals and the estimated channel coefficients $\hat{h}_{n,m}(l)$.

1) Space-Time Soft Decision Feedback TEQ: Define the feedforward and feedback filter matrices, respectively, as

$$\mathbf{F} = [\mathbf{f}_1, \ldots, \mathbf{f}_N] \in \mathcal{C}^{M(K_2+K_1+1)\times N}$$
$$\mathbf{B} = [\mathbf{b}_1, \ldots, \mathbf{b}_N] \in \mathcal{C}^{NK_3\times N}. \quad (19)$$

The ST-SDFE estimate of the kth transmitted symbol vector of the N transducers is given by

$$\hat{\mathbf{s}}_k = \mathbf{F}^H \mathbf{y}^k - \mathbf{B}^H \breve{\mathbf{s}}^k \quad (20)$$

where

$$\breve{\mathbf{s}}^k = [\breve{\mathbf{s}}_{k-K_3}^T, \breve{\mathbf{s}}_{k-K_3+1}^T, \ldots, \breve{\mathbf{s}}_{k-1}^T]^T \in \mathcal{C}^{NK_3\times 1}$$
$$\breve{\mathbf{s}}_k = [\breve{s}_{1,k}, \breve{s}_{2,k}, \ldots, \breve{s}_{N,k}]^T \in \mathcal{C}^{N\times 1}.$$

Here, the sequence $\breve{\mathbf{s}}^k$ is the most recent decisions on every stream, and $\breve{\mathbf{s}}_k$ is the previously equalized symbol vector, with $\breve{s}_{n,k}$ being the soft decision of the kth transmitted symbol from the nth transducer, which is a function of its *a posteriori* LLR obtained at current Turbo iteration. To design the coefficient vectors $\mathbf{f}_n$ and $\mathbf{b}_n$, we use the MMSE metric by minimizing $\mathbf{E}[|\hat{s}_{n,k} - s_{n,k}|^2]$, and the optimum solution is given by

$$\hat{s}_{n,k} = \mathbf{f}_n^H \mathbf{y}^k - \mathbf{b}_n^H \breve{\mathbf{s}}^k$$
$$= \begin{bmatrix} \mathbf{f_n} \\ \mathbf{b}_n \end{bmatrix}^H \begin{bmatrix} \mathbf{y^k} \\ -\breve{\mathbf{s}}^k \end{bmatrix}. \quad (21)$$

Assume that the soft decisions are correct, i.e., $\breve{\mathbf{s}}^k = \mathbf{s}^k$ for all n and k, then the MMSE Winner–Hopf solutions for $\mathbf{f}_n$ and $\mathbf{b}_n$ are solved jointly by

$$\begin{bmatrix} \mathbf{f_n} \\ \mathbf{b}_n \end{bmatrix} = \mathbf{\Psi}^{-1} \mathbf{d}_n \quad (22)$$

where

$$\mathbf{d}_n = \mathbf{E} \begin{bmatrix} \mathbf{y^k} \\ -\breve{\mathbf{s}}^k \end{bmatrix} s_{n,k}^*$$
$$= \mathbf{E} \left[s_{n,k} s_{n,k}^* \right] \begin{bmatrix} [\hat{\mathbf{H}}]_{[NK_3+n]} \\ \mathbf{0} \end{bmatrix} \quad (23)$$

and

$$\mathbf{\Psi} = \mathbf{E} \left(\begin{bmatrix} \mathbf{y^k} \\ -\breve{\mathbf{s}}^k \end{bmatrix} \begin{bmatrix} \mathbf{y^k} \\ -\breve{\mathbf{s}}^k \end{bmatrix}^H \right)$$
$$= \mathbf{E} \left[s_{n,k} s_{n,k}^* \right] \begin{bmatrix} \hat{\mathbf{H}}\hat{\mathbf{H}}^H & -\mathbf{V} \\ -\mathbf{V}^H & \mathbf{I} \end{bmatrix} \quad (24)$$

where $[\cdot]_{[NK_3+n]}$ indicates the (NK_3+n)th column of the estimated channel matrix $\hat{\mathbf{H}}$, and $\mathbf{V} = [[\hat{\mathbf{H}}]_{[1:N:(N-1)K_3]}, \ldots, [\hat{\mathbf{H}}]_{[N:N:NK_3]}]$. Also, $\hat{\mathbf{H}}$ is defined as (18) by replacing the channel coefficients $h_{n,m}(l)$ with the estimated channel coefficients $\hat{h}_{n,m}(l)$. Similar structure is referred in [36]. The highly structured form of $\mathbf{\Psi}$ may be exploited to simplify the calculation of its inverse in (22). Equations (23) and (24) make sense by utilizing the space-time structure of the transmitted symbols, where the $N \times 1$ vector $\mathbf{s}_k$ transmitted at time k is time independent within every individual burst, leading to the diagonal spatial covariance

$$\mathbf{E} \left[\mathbf{s}_k \mathbf{s}_k^H \right] = \frac{P_T}{N} \mathbf{I}_N \quad (25)$$

where P_T is the total average transmit power which is consistent regardless of the transducer number. The expectation is simply

$$\mathbf{E}[s_{n,k} s_{n,k}^*] = \frac{P_T}{N}.$$

Equations (23) and (24) reveal that the feedforward filter vector $\mathbf{f}_n$ and feedback filter vector $\mathbf{b}_n$ are determined solely by the expectation of the current (n,k)th symbol $s_{n,k}$ and the main column of the estimated channel matrix $\hat{\mathbf{H}}$ that covers all the channel coefficients associated with the nth transducer. The computational complexity is greatly reduced since the expectations in calculating $\mathbf{d}_n$ and $\mathbf{\Psi}$ are converted into the symbol power and channel estimates. The filter coefficients $\mathbf{f}_n$ and $\mathbf{b}_n$ can be calculated when equalizing the first symbol of the subblock and keep them fixed in the current subblock to further reduce the computational complexity that involves the matrix inverse of $\mathbf{\Psi}$.

Once the equalizer filters are designed, the received signals are filtered through the equalizer and the SSIC is applied to the first Turbo iteration and beyond, where (21) is revised as

$$\hat{s}_{n,k} = \mathbf{f}_n^H \left(\mathbf{y}^k - \hat{\mathbf{H}}\tilde{\mathbf{s}}^k \right) - \mathbf{b}_n^H \left(\breve{\mathbf{s}}^k - \bar{\mathbf{s}}^k \right) \quad (26)$$

where

$$\tilde{\mathbf{s}}^k = [\bar{\mathbf{s}}_{k-K_2-L+1}^T, \ldots, \bar{\mathbf{s}}_{k-1}^T, \tilde{\mathbf{s}}_{n,k}^T, \bar{\mathbf{s}}_{k+1}^T, \ldots, \bar{\mathbf{s}}_{k+K_1}^T]^T$$
$$\bar{\mathbf{s}}_k = [\bar{s}_{1,k}, \bar{s}_{2,k}, \ldots, \bar{s}_{N,k}]^T$$
$$\tilde{\mathbf{s}}_{n,k} = [\bar{s}_{1,k}, \ldots, \bar{s}_{n-1,k}, 0, \bar{s}_{n+1,k}, \ldots, \bar{s}_{N,k}]^T$$
$$\bar{\mathbf{s}}^k = [\bar{\mathbf{s}}_{k-K_3}^T, \bar{\mathbf{s}}_{k-K_3+1}^T, \ldots, \bar{\mathbf{s}}_{k-1}^T]^T.$$

Here, $\bar{s}_{n,k}$ is the soft estimate of the kth transmitted symbol from the nth transducer, which is a function of its *a priori* LLR at the current Turbo iteration. Note that the *a posteriori* soft decisions $\breve{\mathbf{s}}^k$ used in the feedback filter $\mathbf{b}_n$ are unavailable when $k < K_3$, and we adopt the *a priori* LLR of the corresponding symbols, which may slightly degrade the performance of those symbols.

This article has been accepted for inclusion in a future issue of this journal. Content is final as presented, with the exception of pagination.

6   IEEE JOURNAL OF OCEANIC ENGINEERING

2) Soft Decisions and LLRs Calculation: Instead of using the soft estimated symbols from (26) as the final decision, we proceed to calculate the soft decision of the $\hat{s}_{n,k}$ as the final output, expressed as

$$\breve{s}_{n,k} = \sum_{\chi_q \in \mathcal{S}} \chi_q \Pr(s_{n,k} = \chi_q | \hat{s}_{n,k}) \tag{27}$$

where the *a posteriori* probability $\Pr(s_{n,k} = \chi_q | \hat{s}_{n,k})$ is given by

$$\Pr(s_{n,k} = \chi_q | \hat{s}_{n,k}) = \frac{p(\hat{s}_{n,k} | s_{n,k} = \chi_q) \Pr(s_{n,k} = \chi_q)}{p(\hat{s}_{n,k})} \tag{28}$$

and the *a priori* probability $\Pr(s_{n,k} = \chi_q)$ is computed as

$$\Pr(s_{n,k} = \chi_q) = \prod_{p=1}^{\log_2 Q} \frac{1}{2} \left(1 + \tilde{a}_{q,p} \tanh(L_e^D(c_{n,p}^k)/2) \right) \tag{29}$$

where $\tilde{a}_{q,p}$ is the predetermined bit patterns with $\tilde{a}_{q,p} = 1$ when $a_{q,p} = 0$ and $\tilde{a}_{q,p} = -1$ when $a_{q,p} = 1$. A given constellation point χ_q is mapped to the corresponding bit patterns

$$\mathbf{a}_q = [a_{q,1}, a_{q,2}, \ldots, a_{q,\log_2 Q}]^T.$$

Also, $L_e^D(c_{n,p}^k)$ is the *a priori* LLRs of equalizer which are acquired from the MAP decoder, since the equalized symbols $\hat{s}_{n,k}$ are assumed to be the outputs of an equivalent AWGN channel and follow the Gaussian distribution $\hat{s}_{n,k} \sim \mathcal{CN}(\mu_{n,k} s_{n,k}, \sigma_{n,k}^2)$. Therefore, the conditional probability distribution function of the equalized symbols in (28) is expressed as

$$p(\hat{s}_{n,k} | s_{n,k} = \chi_q) = \frac{1}{\pi \sigma_{n,k}^2} \exp\left(-\rho_{n,q}^k\right) \tag{30}$$

where

$$\rho_{n,q}^k = \frac{|\hat{s}_{n,k} - \mu_{n,k} \chi_q|^2}{\sigma_{n,k}^2}$$

and $\mu_{n,k}$ and $\sigma_{n,k}^2$ are calculated by

$$\mu_{n,k} = \mathbf{f}_n^H \tilde{\mathbf{h}}_n \tag{31a}$$

$$\sigma_{n,k}^2 = \mu_{n,k}(1 - \mu_{n,k}) \tag{31b}$$

respectively, with $\tilde{\mathbf{h}}_n$ being the $(NK_3 + n)$th column of $\hat{\mathbf{H}}$, since we treat the UWA channel as time-invariant during each subblock period N_{sb} whose channel update is unnecessarily performed symbol-wise. Therefore, $\mu_{n,k}$ and $\sigma_{n,k}^2$ are reduced to μ_n and σ_n^2 to save the computation dramatically. Furthermore, the denominator in (28) is computed via the normalization of

$$\sum_{q=1}^{Q} \Pr(s_{n,k} = \chi_q | \hat{s}_{n,k}) = 1.$$

Accordingly, the extrinsic LLRs of the interleaved bits generated from the equalizer are directly calculated by [37]

$$L_e^E(c_{n,p}^k) = \ln$$

$$\times \frac{\sum_{\chi_q : c_{n,p}^k = 0} \exp\left(-\rho_{n,q}^k + \sum_{\forall p, p' \neq p} \tilde{a}_{q,p'} L_e^D(c_{n,p'}^k)/2\right)}{\sum_{\chi_q : c_{n,p}^k = 1} \exp\left(-\rho_{n,q}^k + \sum_{\forall p, p' \neq p} \tilde{a}_{q,p'} L_e^D(c_{n,p'}^k)/2\right)}. \tag{32}$$

which is readily fed back to the MAP decoder as the *a priori* information via deinterleaving operation. After going through the MAP decoder, $L_e^D(c_{n,p}^k)$ is fed back again into the ST-SDFE unit as the *a priori* LLRs for the next Turbo iteration.
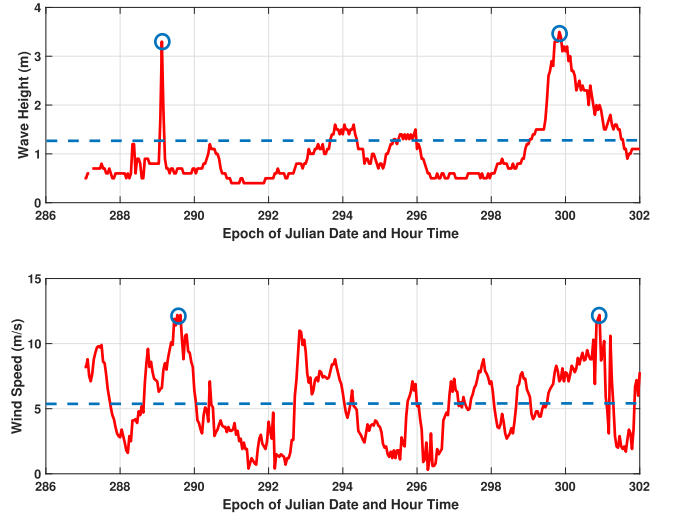

Fig. 4.   Oceanographic and meteorological data in SPACE08. The average wave height and wind speed were 1.25 m and 5.395 m/s labeled by the blue dash–dot line, respectively. Two blue circle marks in each figure denoted the Julian dates 289, 300 and 289, 301, respectively.

IV. EXPERIMENT RESULTS

The proposed MIMO detector was tested by the data of the undersea trial of SPACE08. The merits of the proposed I-SBL CE algorithm are demonstrated via comparison to other channel estimators, such as the MMSE [17], OMP [28], IPNLMS [22], sparse Bayesian algorithm [35] (cited as Bayesian-I), and nonsparse Bayesian algorithm [32] (cited as Bayesian-II). The ST-SDFE structure is also compared with the LC-MMSE linear equalizer [22].

A. Experiment Description

The SPACE08 experiment was conducted in October 2008, by the Woods Hole Oceanographic Institution at the Air-Sea Interaction Tower, two miles south of the coast of Martha's Vineyard, MA, USA, at a sea depth about 15 m. The channel conditions were closely linked with the oceanographic and meteorological data such as wave height and wind speed, as shown in Fig. 4, where the dynamic variations were used as the reference to determine the channel conditions and communication quality. Many descriptions about this sea trial experiment have been provided [17], [22], and we will not repeat the tedious experimental specifications.

In this experiment, QPSK, 8PSK, and 16 QAM signal carrier modulation (SCM) were used with a baseband symbol period of $T_s = 0.1024$ milliseconds (ms). The carrier frequency was $f_c = 13$ kHz. The transmitter filter was a square-root raised cosine filter with the roll-off factor 0.22 and the occupied channel bandwidth 9.7656 kHz. The transmission frame structure of each transducer is illustrated in Fig. 5. The data frame began with a header LFM named LFMB, followed by three SCM packets: QPSK, 8PSK, 16QAM, and ended with a trailing LFM signal named LFME. Zero-padded gaps were inserted between the LFM header and SCM packets, and between the adjacent frames. Each of the SCM packet included an m-sequence of length-511, and a data payload consisting of $N_d = 30\,000$ modulated symbols. The LFM served multiple purposes including the coarse synchronization, carry frequency offset estimation and compensation, and the channel length measurement, attributed to their unique correlation properties. The m-sequence was used for evaluating the channel scattering function, calculating the *a priori* $\mathbf{R}_m^{(0)}$ and $(\sigma^2)^{(0)}$ for the
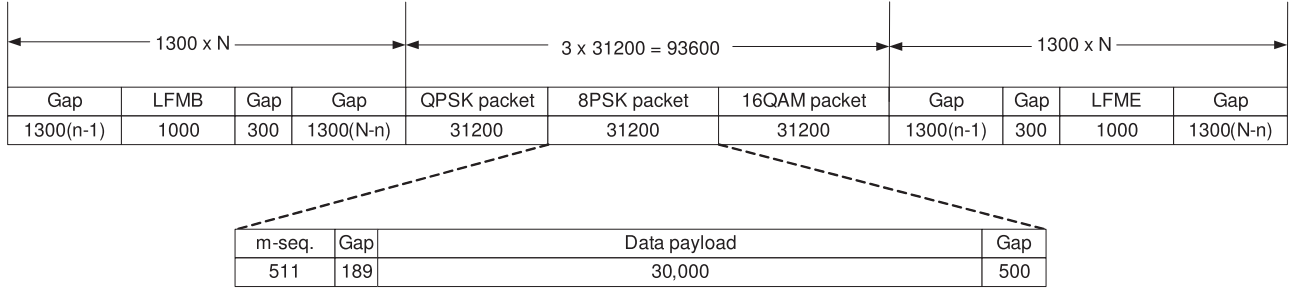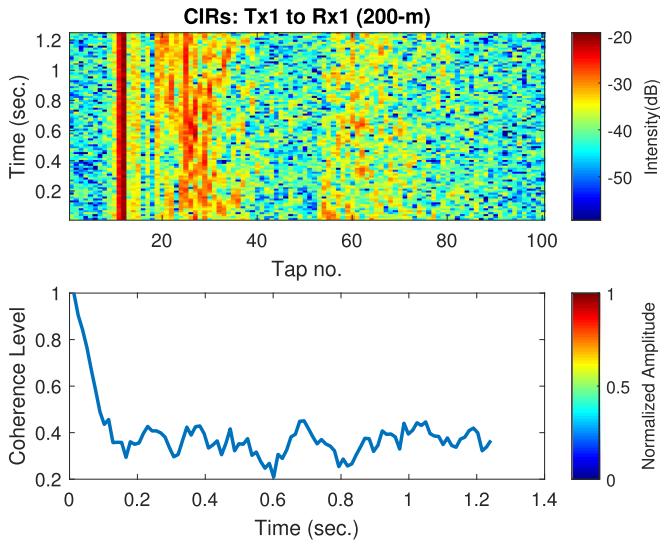
This article has been accepted for inclusion in a future issue of this journal. Content is final as presented, with the exception of pagination.

QIN *et al.*: BAYESIAN ITERATIVE CE AND TEQ FOR MULTIPLE-INPUT–MULTIPLE-OUTPUT UNDERWATER ACOUSTIC COMMUNICATIONS 7

Fig. 5. Burst structure of the nth transmit branch in the SPACE08 experiment.

Fig. 6. Estimated CIR and its coherence time: Packet 1 from transducer 1 (Tx1) to hydrophone 1 (Rx1) at 200-m transmission distance.

TABLE I
PARAMETER SETUP FOR DIFFERENT COMBINATIONS

Modulation	$N \times M$ MIMO	N_b	ξ	R_c (kb/s)
QPSK	2×6	4950	12.12%	17.16
	3×9	3750	16.00%	24.61
	4×12	2550	23.53%	29.87
8PSK	2×6	3750	16.00%	24.61
	3×9	2550	23.53%	33.60
	4×12	1950	30.77%	40.56
16QAM	2×6	2550	23.53%	29.87
	3×9	1950	30.77%	40.56
	4×12	1500	40.00%	46.87

I-SBL channel estimator. An analysis of the channel scattering function with the m-sequence revealed that the maximum Doppler spread of the channel was about 5 Hz. The baseband CIR distribution and the equivalent channel coherence time at 200-m distance are depicted in Fig. 6. The CIRs were time variant, in which the coherence time was used to evaluate the channel variation level. Most of the channel energy was concentrated within 10 ms, corresponding to a channel with an approximated length of 100 taps. The coherence level decreased to 0.4 at 0.125 s, spanning $0.125 \times 9.7656 \approx 1000$ taps. The tap scaling was in terms of the symbol duration $T_s = 0.1024$ ms.

For the two-transducer MIMO scheme, 45 S3, S4 files (200-m transmission distance) and 19 S5, S6 files (1000-m transmission distance) were processed. For the three-transducer MIMO scheme, 19 S5, S6 files were processed. For the four-transducer MIMO scheme, 19 S5, S6 files were processed.

B. Performance Comparison Under Different CE Algorithms

For the proposed CE-based ST-SDFE, we chose $L = 100$, $K_1 = 100$, and $K_2 = 50$. The MMSE, OMP, IPNLMS, Bayesian-I, Bayesian-II, and the proposed I-SBL were tested and compared in terms of the ST-SDFE before the MAP decoder. To ensure the channel coefficients were quasi time invariant, the subblock length, training overhead, and the information rate for all the modulation types and MIMO configurations were selected as shown in Table I, where the corresponding information

rate follows:

$$R_c = 0.5 \times 9.7656 \times (1 - \xi) N \log_2 Q \qquad (33)$$

with $\xi = N_p/N_b$ being the training overhead rate.

A refined N_{sb}-length subblock was selected in case that the corresponding time duration exceeded the channel coherence time. The length of N_p and N_{sb} should be chosen so as to achieve a tradeoff between the detection performance and the transmission efficiency. We expect to track the channel constantly and avoid the signal-to-noise degradation in the equalized symbols at the tail of each subblock N_{sb}. The subblock partition had an overlap, in which the N_{ovlp} symbols at the tail of the previous block were equalized again in the current block. Considering the coherence time as shown in Fig. 6, we set $N_p + N_{sb} \leq 1000$. Without loss of generality, we set $N_{ovlp} = 50$, $N_{sb} = 200$, $N_p = 600$, and a flexible choice of N_b for different MIMO schemes in Table I. Intuitively, when channel conditions are severe, e.g., more transducers induce more CCI (four transducers), ξ needs to be increased.

Other parameter setup for the proposed I-SBL CE algorithm is summarized as

Number of EM iterations per subblock: $T = 2$

The sparseness controlling factor: $\gamma = 2 \times 10^{-6}$

The convergence threshold: $\delta = 10^{-3}$

Initializing the channel coefficients: $\hat{\mathbf{h}}_m^{(0)} = \mathbf{0}$

Initializing the *a priori* $\left(\sigma^2\right)^{(0)}$ and $\mathbf{R}_m^{(0)}$ using m-sequence

This article has been accepted for inclusion in a future issue of this journal. Content is final as presented, with the exception of pagination.

8   IEEE JOURNAL OF OCEANIC ENGINEERING
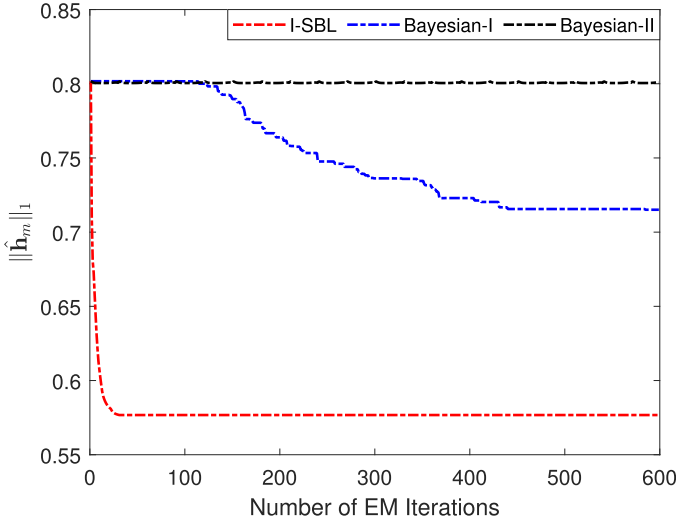

Fig. 7. L_1-norm measurement of the estimated channel links $\hat{\mathbf{h}}_1$ corresponding to the EM iterations of the I-SBL, Bayesian-I, and Bayesian-II algorithms at zero Turbo iteration. Packet 1, 200-m transmission distance with QPSK modulation.
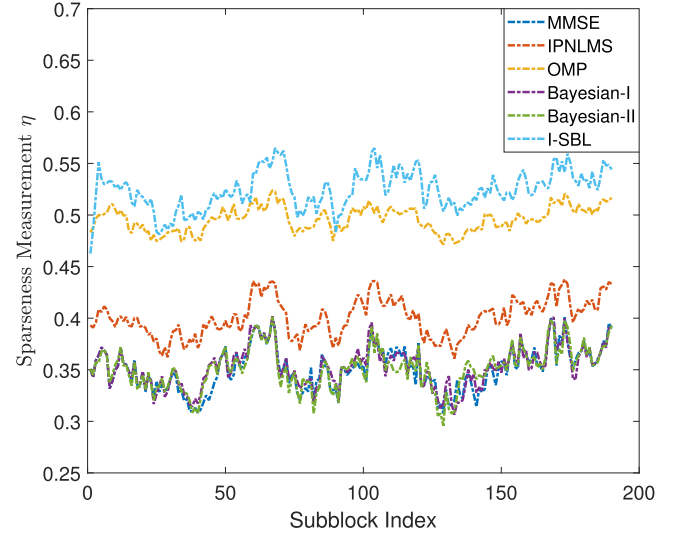

Fig. 8.   Sparseness measurement of the estimated channel links $\hat{\mathbf{h}}_1$ corresponding to the Rx1 at zero Turbo iteration. Packet 1, 200-m transmission distance with QPSK modulation.

Although the channel sparsity of each tested packet was dynamic, we fixed the hyperparameters γ and δ to process all the tested packets. In particular, we chose the hyperparameters as $\gamma = 2 \times 10^{-6}$ and $\delta = 10^{-3}$, because these values were suitable for all the tested packets. In our experience, a larger γ or a smaller δ reinforces the estimated channels to be sparser, but the sensitivity of these hyperparameters to the CE performance is low making the proposed I-SBL robust against the variations in the real channel condition. The reason for the proposed I-SBL CE algorithm achieving excellent performance over the other CE counterparts was its robust parameter update of $\mathbf{h}_m$, $\mathbf{R}_m$, σ^2 and the utilization of the *a priori* estimates $(\sigma^2)^{(0)}$ and $\mathbf{R}_m^{(0)}$. In comparison with the MMSE, OMP, and IPNLMS algorithms, the robust parameter update of the I-SBL enhances the channel tracking by exploring the spatial correlation and sparse nature of the MIMO UWA channels. The utilization of the *a priori* estimates reduces the computational complexity, leads to fast convergence, and enjoys more compact threshold control than the conventional Bayesian algorithms (Bayesian-I and Bayesian-II).

Fig. 7 depicts the L_1-norm measurement of $\mathbf{h}_1$ corresponding to the EM iterations, where all the hyperparameters were the same for all the three Bayesian schemes. Compared with the Bayesian-I and Bayesian-II counterparts, the proposed I-SBL enhanced the channel sparsity and converged at 15th EM iterations which was far less than that of the other two Bayesian channel estimators. In fact, when we increased the EM iterations, the $\|\mathbf{h}_m\|_1$ convergence of the Bayesian-I became unstable, and Bayesian-II showed no sparseness reinforcement. During the data processing, we fixed the maximum EM iteration $T = 2$, which reduced the computational burden significantly, and the I-SBL still performed very well.

We also measured the sparseness of the estimated CIRs by using different channel estimators. The level of sparseness in $\mathbf{h}_m$ is defined as

$$\eta = \frac{NL}{NL - \sqrt{NL}} \left(1 - \frac{\|\mathbf{h}_m\|_1}{\sqrt{NL}\|\mathbf{h}_m\|_2} \right) \qquad (34)$$

where the p-norm is defined by

$$\|\mathbf{h}_m\|_p := \left(\sum_{n=1}^{N} \sum_{l=0}^{L-1} |h_{n,m}(l)|^p \right)^{\frac{1}{p}}. \qquad (35)$$

Different from [22], this article measured the joint channel sparseness of the N transducers whose received signals were projected on the given mth hydrophone simultaneously. A larger η indicates that the estimated channel has sparser structure and the corresponding channel estimator enjoys better sparsity control. For all the six channel estimators, the sparseness of the estimated CIRs at the given channel links $\mathbf{h}_1$ of packet 1, 200-m transmission distance is shown in Fig. 8, which was a representative channel condition during the experiment. Since the MMSE and Bayesian-II criterion enhanced no channel sparsity, η was the smallest ≈ 0.35. Although adopting the channel sparsity, the failure of sparseness in Bayesian-I was due to the slow convergence of γ_l, as we only took two iterations inside the EM algorithm, which was far less than the convergence state as shown in Fig. 8. The IPNLMS algorithm inherently had the capability of sparseness enhancement, and $\eta \approx 0.4$ achieved minor sparseness gain over the MMSE, Bayesian-I and Bayesian-II. For the OMP and I-SBL algorithms, the sparseness η was over 0.45, and the channel sparseness was determined by the hyperparameters artificially, e.g., for the I-SBL, we restrained the channel sparseness via γ. However, the estimated channel sparseness is unable to determine the channel tracking capability as the true channel state was unavailable *a priori*. Therefore, Fig. 8 only demonstrates that the I-SBL can achieve better channel sparseness control than the other counterparts. Alternately, Fig. 9 depicts the signal prediction error measurement [28] of the equalized symbols $\hat{s}_{n,k}$ to evaluate the CE performance straightforwardly with ST-SDFE, corresponding to Fig. 8. The smaller the signal prediction error is, the better performance the channel estimator will have. Combined with Figs. 8 and 9, some analysis is drawn.

1) The channel in SPACE08 was time varying, leading to a time-varying estimated CIR, so it made perfect sense that the sparseness curves of the estimated CIRs were also time varying and almost had the same tendency for all the channel estimators under test.
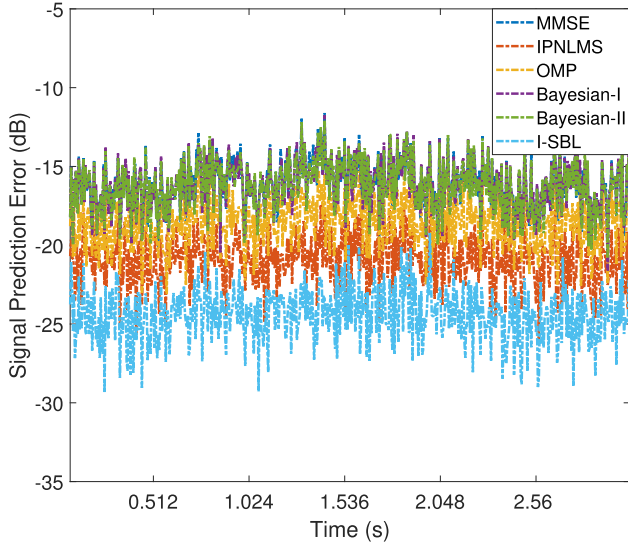
This article has been accepted for inclusion in a future issue of this journal. Content is final as presented, with the exception of pagination.

QIN *et al.*: BAYESIAN ITERATIVE CE AND TEQ FOR MULTIPLE-INPUT–MULTIPLE-OUTPUT UNDERWATER ACOUSTIC COMMUNICATIONS 9

Fig. 9. Average signal prediction error of $\hat{s}_{n,k}$ in decibels (dB), 2×6 MIMO transmission at zero Turbo iteration. Packet 1, 200-m transmission distance with QPSK modulation.
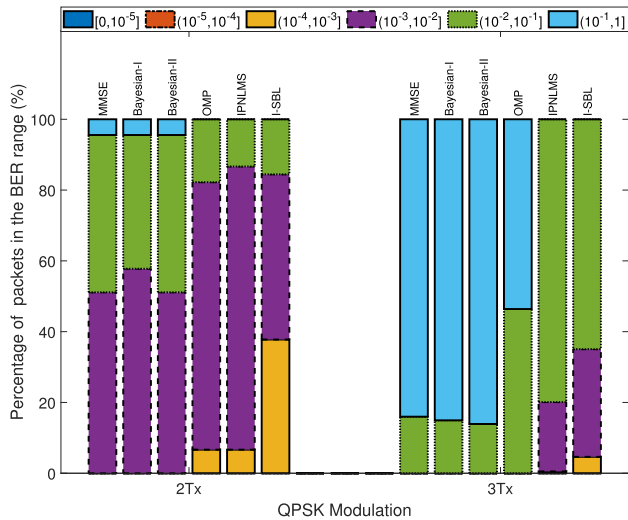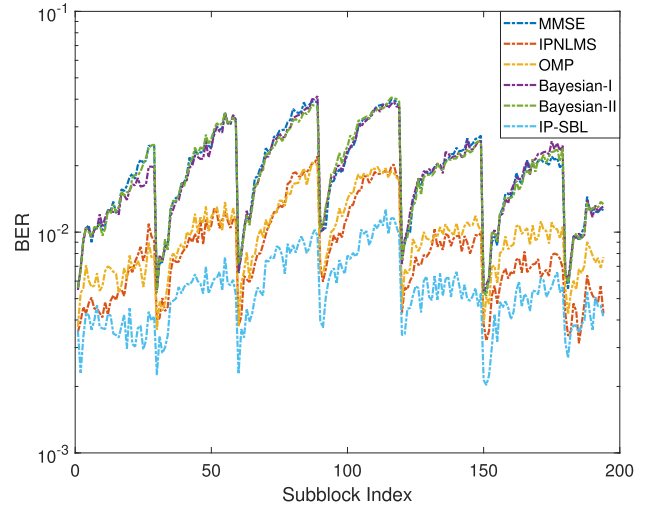

Fig. 11. Averaged BER corresponding to the subblocks of 2×6 MIMO transmission at zero Turbo iteration before MAP decoder, with QPSK modulation.

Fig. 10. Results of 2×6 and 3×9 MIMO transmission at zero Turbo iteration before MAP decoder, with QPSK modulation.

2) The proposed I-SBL had both the sparsest estimated CIR and the best estimate performance.
3) The estimated channel sparseness was insufficient to determine the estimation performance, e.g., the OMP had sparser estimated CIR but worse performance than that of IPNLMS. Therefore, excessive sparseness will induce bias in the estimate process for the L_p-norm algorithms such as OMP.

To better emphasize the performance gain brought by the proposed I-SBL CE algorithm, we also compared the BER benchmark of using different CE algorithms before the MAP decoder, which excludes the performance gain from the powerful MAP decoder. For the QPSK modulation with 2×6 and 3×9 MIMO schemes, the experimental results are shown in Fig. 10, in terms of the percentage of all the packets that fall in the specified BER ranges at the zero Turbo iteration using ST-SDFE. For the 2×6 MIMO system, the MMSE, Bayesian-I, and Bayesian-II channel estimators performed worse for the fast

time-varying channels, thus resulting in the largest percentage of packets with unsatisfactory BER $> 10^{-2}$. The reason for the bad performance of Bayesian-I and Bayesian-II was attributed to the slow parameter convergence and vulnerable channel sparsity control. In contrast, for the I-SBL channel estimator, most of the packets achieved satisfactory BER $\leq 10^{-2}$. Specifically, 38.8% of the packets achieved BER $\leq 10^{-3}$. For the 3×9 MIMO system, as the number of transducers increased, the BER performance became worse due to the more CCI but insufficient training symbols. Nevertheless, the I-SBL channel estimator still performed the best among the six channel estimators. Fig. 11 gives the averaged BER corresponding to each subblock for the 2×6 MIMO system. Since the 2×6 MIMO system updated the CE in the training mode every 30 subblocks, the BER performance was periodical due to the error propagation. The I-SBL still had the strongest channel tracking capability, proving that the results in Fig. 10 were valid. As a preliminary conclusion, the proposed I-SBL solves the matrix inverse for channel estimating better than the other counterparts and induces less singularity when increasing the MIMO size.

C. BER Comparison of the ST-SDFE TEQ and LC-MMSE TEQ

The BER performance comparison of the proposed ST-SDFE-based TEQ and LC-MMSE TEQ with different MIMO sizes and modulation schemes is presented next. First, results of QPSK 2×6 MIMO are listed in Table II, where the number of packets that achieved zero BER is shown for each Turbo iteration. For the 200-m transmission, all 45 QPSK packets achieved zero BER with no more than one Turbo iteration for the proposed ST-SDFE. In comparison, the LC-MMSE equalizer took two Turbo iterations to achieve BER-free-packet. For the 1000-m transmission, 18 out of 19 QPSK packets achieved zero BER after one Turbo iteration when using the ST-SDFE, while 16 QPSK packets achieved zero BER when using the LC-MMSE equalizer with the same number of Turbo iterations.

For the 8PSK and 16QAM modulation with 2×6 MIMO, the experimental results comparison of the LC-MMSE equalizer and ST-SDFE with I-SBL channel estimators are illustrated in Fig. 12, in terms of the percentage of packets that fall in the specified BER ranges after five Turbo iterations. For the higher order modulation schemes, the ST-SDFE outperformed the LC-MMSE equalizer, leading to 57.9%

This article has been accepted for inclusion in a future issue of this journal. Content is final as presented, with the exception of pagination.

10   IEEE JOURNAL OF OCEANIC ENGINEERING

TABLE II
BER BENCHMARK OF QPSK 2×6 MIMO USING LC-MMSE TEQ
AND ST-SDFE TEQ

Range	# of iter	# of packets achieved zero BER	
		(LC-MMSE)	(ST-SDFE)
200 m	0	25	31
	1	18	14
	2	2	-
	3	-	-
	4	-	-
	5	-	-
	Total	45	45
1000 m	0	12	16
	1	4	2
	2	1	0
	3	0	1
	4	0	-
	5	0	-
	Total	17	19

Fig. 13.   Results of the 3×9 MIMO 1000-m transmission using the LC-MMSE equalizer and ST-SDFE after 5 Turbo iterations.

Fig. 12.   Results of the 2×6 MIMO 1000-m transmission using the LC-MMSE equalizer and ST-SDFE after five Turbo iterations.
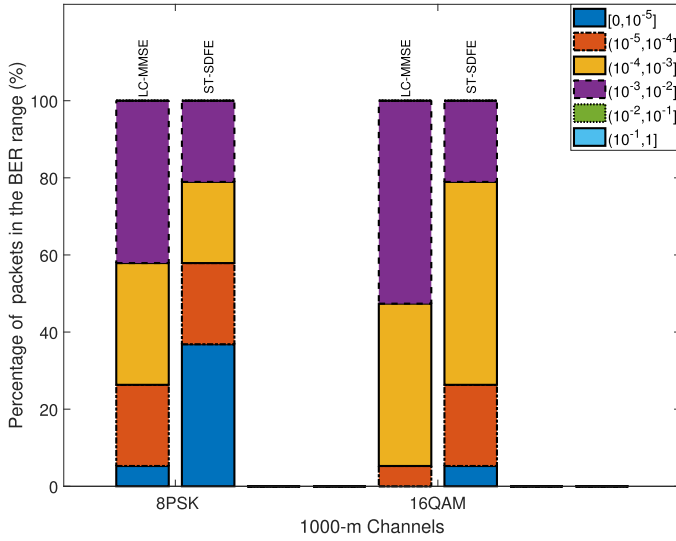

Fig. 14.   Results of the 4×12 MIMO 1000-m transmission using the LC-MMSE equalizer and ST-SDFE after five Turbo iterations.

percentage of the packets achieving BER $\leq 10^{-4}$ with the 8PSK modulation scheme.

For the 3×9 MIMO 1000-m transmission, the experimental results are shown in Fig. 13. The overall BER performance was largely degraded due to the severe channel links from the third transducer to the received hydrophones compared with the 2×6 MIMO scheme. Although we increased the training overhead ξ, the performance gain was limited and most of the error bits originated from the data stream of the third transducer. Moreover, the 16QAM modulation scheme achieved better BER performance than the 8PSK scheme with the LC-MMSE equalizer, which was not reasonable in intuition. Herein, we give the explanation that the LLR calculation for the LC-MMSE equalizer was not stable due to the severe channel links from the third transducer. Nevertheless, the ST-SDFE still outperformed the LC-MMSE equalizer.

For the 4×12 MIMO 1000-m transmission, the experimental BER comparison results are illustrated in Fig. 14. A larger training overhead ξ in Table I was chosen with $N_b = 1950, 1500$ for the 8PSK and 16QAM, respectively. Since ξ was sufficient enough to track the dynamic UWA

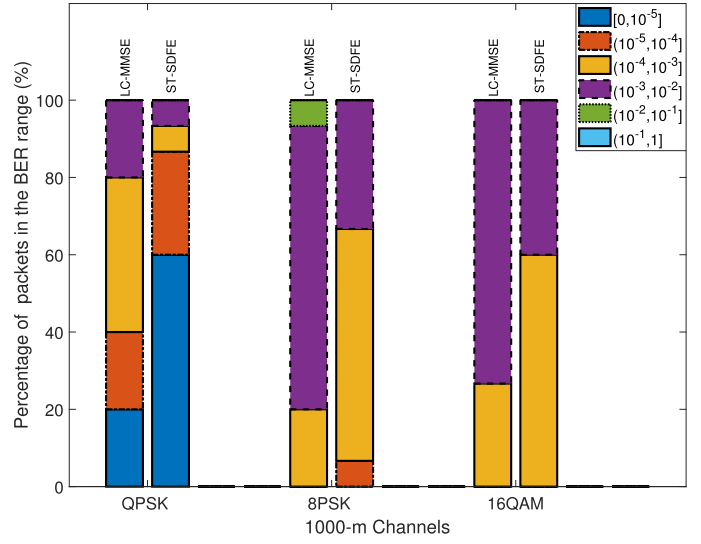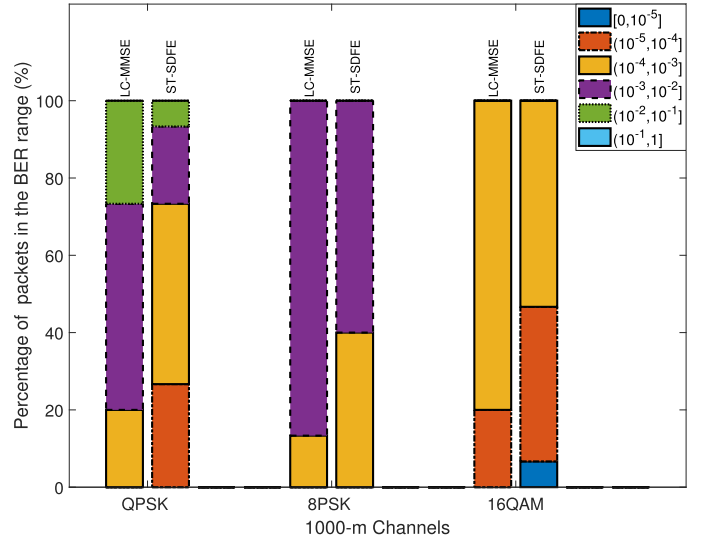channels, the BER benchmark of 16QAM in 4×12 MIMO scheme outperformed 8PSK and 16QAM in the 3×9 MIMO scheme, and even performed better than QPSK and 8PSK in the 4×12 MIMO scheme.

V. COMPUTATIONAL COMPLEXITY ANALYSIS

The computational complexity of the six channel estimators is listed in Table III in terms of the number of multiplications, where $\beta_{\max}$ denotes the round of training sequence reuse in [22]. The computational complexity of the block-wise MMSE, OMP, Bayesian-I, Bayesian-II, and I-SBL channel estimators was on the order of $\mathcal{O}((NL)^3)$, and was on the order of $\mathcal{O}(NL)$ for IPNLMS. The given parameters were set as $\beta_{\max} = 5$, $L = 100$, $N = 2$, $M = 6$, $N_p = 600$ and $T = 2$. Since the channel sparsity was nonuniform, without loss of generality, we fixed $L_\alpha = 50$, and the number of million multiplications required for the six channel estimators for each subblock processing is shown in

This article has been accepted for inclusion in a future issue of this journal. Content is final as presented, with the exception of pagination.

QIN *et al.*: BAYESIAN ITERATIVE CE AND TEQ FOR MULTIPLE-INPUT–MULTIPLE-OUTPUT UNDERWATER ACOUSTIC COMMUNICATIONS 11

TABLE III
COMPUTATIONAL COMPLEXITY OF THE CHANNEL ESTIMATORS

Channel estimator	Explicit number of multiplications Per subblock detection
MMSE	$(NL)^3/2 + NL(N_p - L + 1)(NL + M)$
IPNLMS	$\beta_{max} M N_p (5NL + 3)$
OMP	$NL(N_p - L + 1) + \sum_{\alpha=1}^{NL_\alpha} \left(\alpha^3/2 + \alpha(N_p - L + 1)(\alpha + M + 1) \right)$
Bayesian-I	$2TNL_\alpha \left((N_p - L + 1)(M + 2NL_\alpha) + (NL_\alpha)^2 \right)$
Bayesian-II	$(N_p - L + 1) \left((N_p - L + 1) + T \left(5NL(N_p - L + 1) + 2NLM + (N_p - L + 1)^2 \right) \right)$
I-SBL	$T \left(N^2 L_\alpha + N^3/2 + (NL_\alpha) \left((NL_\alpha)^2 + (NL_\alpha + 1)(N_p - L + 1)M \right) \right)$

TABLE IV
DETAILED NUMBER OF MILLION MULTIPLICATIONS OF THE CHANNEL
ESTIMATORS FOR EACH SUBBLOCK PROCESSING ($\beta_{MAX} = 5$, $L = 100$, $N_p = 600$, $T = 2$, $L_\alpha = 50$)

MIMO	2×6	3×9	4×12
MMSE CE	24.64	59.94	114.56
IPNLMS CE	18.05	40.58	72.11
OMP CE	200.08	690.29	1679.15
Bayesian-I CE	45.28	106.39	197.13
Bayesian-II CE	756.16	1010.17	1265.38
I-SBL CE	62.72	211.01	499.37

Table IV. When increasing the MIMO size, the number of multiplications required for the MMSE channel estimator was 1.5 times as many as that needed for the IPNLMS channel estimator. For the OMP and Bayesian-II channel estimators, the complexity increased rapidly with larger MIMO size, which was unpromising for the MIMO CE. For the Bayesian-I channel estimators, while enjoying relatively less computation than the I-SBL channel estimators, it was still not preferable due to the slow L_1 convergence of $\mathbf{h}_m$ as shown in Fig. 7, and also the tedious hyperparameter control. For the proposed I-SBL channel estimator, the complexity was acceptable in terms of performance gain over the block-wise MMSE channel estimator.

VI. CONCLUSION

An effective MIMO detector has been proposed that uses the I-SBL algorithm for CE and ST-SDFE for the TEQ. Experimental results have demonstrated that the I-SBL channel estimator achieved faster parameter convergence and better sparsity control than the conventional Bayesian and OMP algorithms. While sacrificing acceptable complexity compared with IPNLMS, I-SBL had better estimation accuracy in terms of the BER performance than the IPNLMS, MMSE, OMP, and conventional Bayesian channel estimators. Experimental results have also verified that ST-SDFE achieved an order of magnitude improvement of BER performance over that using the LC-MMSE Turbo equalizer.

REFERENCES

[1] D. B. Kilfoyle and A. B. Baggeroer, "The state of the art in underwater acoustic telemetry," *IEEE J. Ocean. Eng.*, vol. 25, no. 1, pp. 4–27, Jan. 2000.

[2] B. Song and J. Ritcey, "Spatial diversity equalization for MIMO ocean acoustic communication channels," *IEEE J. Ocean. Eng.*, vol. 21, no. 4, pp. 505–512, Oct. 1996.

[3] S. Gray, J. C. Preisig, and D. Brady, "Multiuser detection in a horizontal underwater acoustic channel using array observations," *IEEE Trans. Signal Process.*, vol. 45, no. 1, pp. 148–160, Jan. 1997.

[4] D. B. Kilfoyle, J. C. Preisig, and A. B. Baggeroer, "Spatial modulation experiments in the underwater acoustic channels," *IEEE J. Ocean. Eng.*, vol. 30, no. 2, pp. 406–415, Apr. 2005.

[5] S. Roy, T. M. Duman, M. McDonald, and J. G. Proakis, "High-rate communication for underwater acoustic channels using multiple transmitters and space-time coding: Receiver structures and experimental results," *IEEE J. Ocean. Eng.*, vol. 32, no. 3, pp. 663–688, Jul. 2007.

[6] J. Ling, K. Zhao, J. Li, and M. L. Nordenvaad, "Multi-input multi-output underwater acoustic communications over sparse and frequency modulated acoustic channels," *J. Acoust. Soc. Amer.*, vol. 130, no. 1, pp. 3067–3078, Jul. 2011.

[7] S. E. Cho, H. C. Song, and W. S. Hodgkiss, "Successive interference cancellation for underwater acoustic communications," *IEEE J. Ocean. Eng.*, vol. 36, no. 4, pp. 490–501, Oct. 2011.

[8] J. Zhang and Y. R. Zheng, "Frequency-domain Turbo equalization with soft successive interference cancellation for single carrier MIMO underwater acoustic communications," *IEEE Trans. Wireless Commun.*, vol. 10, no. 9, pp. 2872–2882, Sep. 2011.

[9] A. Rafati, H. Lou, and C. Xiao, "Soft-decision feedback Turbo equalization for LDPC-coded MIMO underwater acoustic communications," *IEEE J. Ocean. Eng.*, vol. 39, no. 1, pp. 90–99, Jan. 2014.

[10] Z. Chen, J. Wang, and Y. R. Zheng, "Frequency-domain Turbo equalization with iterative channel estimation for MIMO underwater acoustic communications," *IEEE J. Ocean. Eng.*, vol. 42, no. 3, pp. 711–721, Jul. 2017.

[11] W. Duan, J. Tao, and Y. R. Zheng, "Efficient adaptive Turbo equalization for multiple-input–multiple-output underwater acoustic communications," *IEEE J. Oecan. Eng.*, vol. 43, no. 3, pp. 792–804, Jul. 2018.

[12] F. Qu, Z. Wang, and L. Yang, "Differential orthogonal space-time block coding modulation for time-variant underwater acoustic channels," *IEEE J. Ocean. Eng.*, vol. 42, no. 1, pp. 188–198, Jan. 2017.

[13] B. Li *et al.*, "MIMO-OFDM for high-rate underwater acoustic communications," *IEEE J. Oecan. Eng.*, vol. 34, no. 4, pp. 634–644, Oct. 2009.

[14] P. C. Carrascosa and M. Stojanovic, "Adaptive channel estimation and data detection for underwater acoustic MIMO-OFDM systems," *IEEE J. Oecan. Eng.*, vol. 35, no. 3, pp. 635–646, Jul. 2010.

[15] J. Tao, "DFT-precoded MIMO OFDM underwater acoustic communications," *IEEE J. Oecan. Eng.*, vol. 43, no. 3, pp. 805–819, Jul. 2018.

[16] J. W. Choi, R. J. Drost, A. C. Singer, and J. C. Preisig, "Iterative multichannel equalization and decoding for high frequency underwater acoustic communications," in *Proc. IEEE Sensor Array Multichannel Signal Process. Workshop*, 2008, pp. 127–130.

This article has been accepted for inclusion in a future issue of this journal. Content is final as presented, with the exception of pagination.

12   IEEE JOURNAL OF OCEANIC ENGINEERING

[17] J. Tao, Y. R. Zheng, C. Xiao, and T. C. Yang, "Robust MIMO underwater acoustic communications using Turbo block decision-feedback equalization," *IEEE J. Oecan. Eng.*, vol. 35, no. 4, pp. 948–960, Oct. 2010.

[18] S. Haykin, *Adaptive Filter Theory*. 4th ed. Englewood Cliffs, NJ, USA: Prentice-Hall, 2002, ch. 5/6.

[19] J. Benesty and S. L. Gay, "A improved PNLMS algorithm," in *Proc. IEEE Int. Conf. Acoust., Speech, Signal Process.*, 2002, pp. 1881–1884.

[20] D. L. Duttweiler, "Proportionate normalized least-mean-squares adaptation in echo cancelers," *IEEE Trans. Speech, Audio Process.*, vol. 8, no. 5, pp. 505–518, Sep. 2000.

[21] K. Pelekanakis and M. Chitre, "Comparison of sparse adaptive filters for underwater acoustic channel equalization/estimation," in *Proc. IEEE Int. Conf. Commun. Syst.*, 2010, pp. 395–399.

[22] Z. Yang and Y. R. Zheng, "Iterative channel estimation and Turbo equalization for multiple-input–multiple-output underwater acoustic communications," *IEEE J. Oecan. Eng.*, vol. 41, no. 1, pp. 232–242, Jan. 2016.

[23] I. F. Gorodnitsky and B. D. Rao, "Sparse signal reconstruction from limited data using FOCUSS: A re-weighted minimum norm algorithm," *IEEE Trans. Signal Process.*, vol. 45, no. 3, pp. 600–616, Mar. 1997.

[24] S. Boyd and L. Vandenberghe, *Convex Optimization*. Cambridge, U.K.: Cambridge Univ. Press, 2004, ch. 6.

[25] W. Zeng and W. Xu, "Fast estimation of sparse doubly spread acoustic channels," *J. Acoust. Soc. Amer.*, vol. 131, no. 1, pp. 303–317, Jan. 2012.

[26] S. F. Cotter and B. D. Rao, "Sparse channel estimation via matching pursuit with application to equalization," *IEEE Trans. Commun.*, vol. 50, no. 3, pp. 374–377, Mar. 2002.

[27] S. G. Mallat and Z. Zhang, "Matching pursuits with time-frequency dictionaries," *IEEE Trans. Signal Process.*, vol. 41, no. 12, pp. 3397–3415, Dec. 1993.

[28] W. Li and J. C. Presig, "Estimation of rapidly time-varying sparse channels," *IEEE J. Oecan. Eng.*, vol. 32, no. 4, pp. 927–939, Oct. 2007.

[29] C. R. Berger and S. Zhou, "Sparse channel estimation for multicarrier underwater acoustic communication: From subspace methods to compressed sensing," *IEEE J. Oecan. Eng.*, vol. 58, no. 3, pp. 1708–1721, Mar. 2010.

[30] J. Ling, T. Yardibi, J. Li, M. L. Nordenvaad, H. He, and K. Zhao, "On Bayesian channel estimation and FFT-based symbol detection in MIMO underwater acoustic communications," *IEEE J. Oecan. Eng.*, vol. 39, no. 1, pp. 59–73, Jan. 2014.

[31] P. Gerstoft, C. F. Mecklenbrauker, A. Xenaki, and S. Nannuru, "Multi-snapshot sparse Bayesian learning for DOA," *IEEE Signal Process. Lett.*, vol. 23, no. 10, pp. 1469–1473, Oct. 2016.

[32] K. L. Gemba, S. Nannuru, P. Gerstoft, and W. S. Hodgkiss, "Multi-frequency sparse Bayesian learning for robust matched field processing," *J. Acoust. Soc. Amer.*, vol. 141, no. 5, pp. 3411–3420, May 2017.

[33] Z. Zhang and B. D. Rao, "Sparse signal recovery with temporally correlated source vectors using sparse Bayesian learning," *IEEE J. Sel. Topics Signal Process.*, vol. 5, no. 5, pp. 912–926, Sep. 2011.

[34] M. E. Tipping and B. D. Rao, "Sparse Bayesian learning and the relevance vector machine," *J. Mach. Learn. Res.*, vol. 1, pp. 211–244, 2004.

[35] D. P. Wipf and B. D. Rao, "An empirical Bayesian strategy for solving the simultaneous sparse approximation problem," *IEEE Trans. Signal Process.*, vol. 55, no. 7, pp. 3704–3716, Jul. 2007.

[36] A. Lozano and C. Papadias, "Layered space-time receivers for frequency-selective wireless channels," *IEEE Trans. Commun.*, vol. 50, no. 1, pp. 65–73, Jan. 2002.

[37] A. Rafati, H. Lou, and C. Xiao, "Low-complexity soft-decision feedback Turbo equalization for MIMO systems with multilevel modulations," *IEEE Trans. Veh. Technol.*, vol. 60, no. 7, pp. 3218–3227, Sep. 2011.

Xiangzhao Qin (S'18) received the B.S. degree in underwater acoustic engineering from Harbin Engineering University, Harbin, China, in 2015. He is currently working toward the Ph.D. degree in marine information and engineering with Ocean College, Zhejiang University, Zhoushan, China.

He is currently a Visiting Student with Lehigh University, Bethlehem, PA, USA. His research interests include underwater acoustic communications and networking, and acoustic signal processing.

Fengzhong Qu (S'07–M'10–SM'15) received the B.S. and M.S. degrees from Zhejiang University, Hangzhou, China, in 2002 and 2005, respectively, both in electrical engineering, and the Ph.D. degree in electrical and computer engineering from the Department of Electrical and Computer Engineering, University of Florida, Gainesville, FL, USA, in 2009.

From 2009 to 2010, he was an Adjunct Research Scholar with the Department of Electrical and Computer Engineering, University of Florida. Since 2011, he has been with the Ocean College, Zhejiang University, Zhoushan, China, where he is currently a Professor and Associate Chair of the Institute of Ocean Sensing and Networking. His current research interests include underwater acoustic communications and networking, wireless communications, signal processing, and intelligent transportation systems.

Dr. Qu is an Associate Editor for the IEEE TRANSACTIONS ON INTELLIGENT TRANSPORTATION SYSTEMS and *IET Communications and China Communications*.

Yahong Rosa Zheng (M'03–SM'07–F'15) received the B.S. degree in electrical engineering from the University of Electronic Science and Technology of China, Chengdu, China, in 1987, the M.S. degree in electrical engineering from Tsinghua University, Beijing, China, in 1989, and the Ph.D. degree in electrical and computer engineering from Carleton University, Ottawa, ON, Canada, in 2002.

From 2003 to 2005, she was an NSERC Postdoctoral Fellow with the University of Missouri, Columbia, MO, USA. From 2005 to 2018, she was the Faculty Member with the Department of Electrical and Computer Engineering, Missouri University of Science and Technology, Rolla, MO, USA, where she held the Wilkens' Missouri Telecommunications Endowed Professor position for 2017–2018. She joined Lehigh University, Bethlehem, PA, USA, in August 2018, as a Professor with the ECE Department. Her research interests include underwater cyber-physical systems, real-time embedded systems and signal processing, wireless communications, and wireless sensor networks.

Dr. Zheng has served as a Technical Program Committee Member for many IEEE international conferences. She served as an Associate Editor for the IEEE TRANSACTIONS ON WIRELESS COMMUNICATIONS (2006–2008) and the IEEE TRANSACTIONS ON VEHICULAR TECHNOLOGY (2008–2016). Since 2016, she has been an Associate Editor for the IEEE JOURNAL OF OCEANIC ENGINEERING. She was the recipient of an NSF faculty CAREER award in 2009. Since 2015, she has been a Distinguished Lecturer of the IEEE Vehicular Technology Society.